Experimental and Molecular Pathology 140 (2024) 104938

Contents lists available at ScienceDirect

Experimental and Molecular Pathology

journal homepage: www.elsevier.com/locate/yexmp

Histomorphological scoring of murine colitis models: A practical guide for the evaluation of colitis and colitis-associated cancer

Marianne Remke [a,b,c,*], Tanja Groll [a,b], Thomas Metzler [a,b], Elisabeth Urbauer [d], Janine Kövilein [d], Theresa Schnalzger [e], Jürgen Ruland [e], Dirk Haller [d], Katja Steiger [a,b,c]

[a] Institute of Pathology, School of Medicine and Health, Technical University of Munich, Trogerstr. 18, 81675 Munich, Germany
[b] Comparative Experimental Pathology, School of Medicine and Health, Technical University of Munich, Trogerstr. 18, 81675 Munich, Germany
[c] Member of the German Cancer Consortium (DKTK), Partner Site Munich, Munich, Germany
[d] Chair of Nutrition and Immunology, Technical University of Munich, Gregor-Mendel-Str. 2, 85354 Freising, Germany
[e] Institute of Clinical Chemistry and Pathobiochemistry, School of Medicine and Health, Technical University of Munich, Ismaninger Str. 22, 81675 Munich, Germany

ARTICLE INFO

Keywords:
Experimental pathology
Inflammatory bowel diseases
Inflammation
Animal models

ABSTRACT

Background and aims: Histomorphology is a powerful and cost-efficient tool for evaluating inflammatory and neoplastic conditions. Inflammatory bowel disease (IBD) is a widespread condition with globally rising incidences, and a lot of research is done to better understand the pathogenesis of IBD and to identify potential therapeutic approaches. However, standardized and reproducible scores for the histomorphological evaluation of murine IBD models are lacking. Therefore, we aimed to develop an easy-to-use and reproducible score for standardized assessment of colitis and associated cancer models.

Methods: In this study, samples from three different colitis models with and without associated cancer formation were analyzed to develop a universal, robust, and reproducible score for the grading of murine colitis models using the following three parameters: 1. Extent of leucocyte infiltration, 2. Tissue damage, 3. Architectural disruption of the mucosa.

Results: A scoring system was established for different kinds of colitis models (genetically induced enterocolitis, genetically induced metabolic injury, and chemically induced colitis-associated cancer) and all stages of the disease, from mild inflammatory changes to severe inflammation with neoplastic changes as the extreme extent of IBD. The scoring scheme is easy to use, can easily be learned, and proves to have a high interrater reliability.

Conclusions: We propose a robust histological scoring system for the assessment of murine colitis and colitis-associated cancer models, giving more researchers access to conclusive and reliable histological assessment.

1. Introduction

The prevalence of inflammatory bowel diseases (IBD), including Crohn's disease and ulcerative colitis, is rising globally. While the age-standardized prevalence rate of IBD was 79.5 (75.9–83.5) per 100,000 population in the 1990s, it increased to 84.3 (79.2–89.9) per 100,000 population in 2017 (GBD 2017 Inflammatory Bowel Disease Collaborators., 2020). It is generally assumed that genetics and malfunction of the immune system are essential factors in the pathogenesis of IBD (Chu et al., 2016; Jostins et al., 2012; Khor et al., 2011), with diet and stress also playing a role (Charlebois et al., 2016; Wang et al., 2019; Wong et al., 2016). However, the exact cause of IBD remains unknown (Mentella et al., 2020). Therefore, numerous animal models have been developed to gain a deeper understanding of the pathophysiology of IBD. Most commonly used are chemically induced models, adoptive T cell transfer models of colitis, congenital mutant, and genetically engineered models (Baydi et al., 2021). Dextran sodium sulfate (DSS), Azoxymethane (AOM)/Dextran sodium sulfate (DSS), and 2,4,6-Trinitrobenzenesulfonic acid (TNBS) are widely used to chemically induce intestinal inflammation (for TNBS and DSS) or colitis-associated cancer

Abbreviations: AOM/DSS, Azoxymethane/Dextran sodium sulfate; DSS, Dextran sodium sulfate; FFPE, Formalin-fixed paraffin-embedded; H&E, Hematoxylin & Eosin; IBD, Inflammatory bowel disease; IEC, Intestinal epithelial cells; IEL, Intraepithelial lymphocyte; MT-UPR, Mitochondrial unfolded protein response; PAS-AB, Periodic acid Schiff - Alcian blue; SIHUMI, Simplified Human Intestinal Microbiota; WT, Wild type.

* Corresponding author at: Institut für Pathologie TU München, Trogerstraße 18, 81675 München, Germany.
E-mail address: Marianne.Remke@tum.de (M. Remke).

https://doi.org/10.1016/j.yexmp.2024.104938
Received 10 May 2024; Received in revised form 19 September 2024; Accepted 4 October 2024
Available online 16 October 2024

(for AOM/DSS) (Waldner and Neurath, 2009). Genetic modifications resulting in an inflammatory phenotype often target genes of the innate immune system, including myeloid and epithelial cell mechanisms (Saez et al., 2023) or the effector response of the adaptive immune system, especially regulatory T-cell response (Geremia et al., 2014; Schirmer et al., 2019). Furthermore, the transfer of T-helper cells into a lymphopenic host can induce colitis (Maschmeyer et al., 2021).

Pro-inflammatory factors and therapeutic effects are monitored by various, often cost-intensive methods at cellular or molecular levels. Although histomorphology is a powerful and cost-efficient tool in the evaluation of intestinal inflammation, only a few research groups take advantage of it as pathologists with expertise in comparative pathology are not readily available (Steiger et al., 2019). There are few guidelines for the histomorphological evaluation of intestinal inflammation in mouse models (Erben et al., 2014; Katakura et al., 2005), however, none of these cover the entire disease spectrum, including the development of carcinomas as a late consequence of IBD. Additionally, they usually refer to only one specific type of mouse model and are not directly transferable to other models. One approach to improve the availability of histomorphological scoring is computer-assisted analysis. Artificial intelligence-based algorithms have already been successfully employed in numerous studies (Iacucci et al., 2023; Peyrin-Biroulet et al., 2024; Uchikov et al., 2024), but these algorithms cover only parts of the disease spectrum (e.g., infiltration by neutrophil granulocytes as a measure of disease activity or detection of neoplastic changes), and most algorithms were not established for murine tissue but for the use in human tissue. However, the morphology in mouse models may well differ from the morphology in human samples. For example, neutrophil granulocytes have a different nuclear appearance in mice than in humans (Pillay et al., 2013). Therefore, the automated, computer-assisted evaluation of histological sections can make histomorphological analysis more efficient and accurate but cannot replace multidimensional assessment by a pathologist or an experienced rater (Cheng et al., 2021; Yoshida and Kiyuna, 2021).

Therefore, we generated an easy-to-use and universal guide for the histomorphological scoring of murine colitis, which covers the whole disease spectrum and can be applied to all kinds of colitis models, including colitis-associated cancer models, allowing the comparison of different models. The grading scheme we developed can be applied without profound histopathological experience. This contributes to an efficient use of resources in the department of pathology and conserves valuable resources for processes that require a pathologist's assessment, such as the characterization of new models, the accurate interpretation and integration of different histopathological methods, or the design of appropriate studies. The score is intended for use in murine colitis models and for research purposes only.

In general, inflammation is a non-specific reaction of the body to eliminate the noxious agent and repair the damage done (Medzhitov, 2008, 2010; Weiss, 2008). Histologically, it is characterized by an immune cell infiltrate, tissue damage, and reactive tissue changes. As a late consequence, chronic inflammation can result in tumorigenesis (Singh et al., 2019). The risk of colorectal cancer for patients with IBD, for example, increases by approximately 1.0 % yearly, 8–10 years after diagnosis (Kappelman et al., 2014; Munkholm, 2003). To cover the whole spectrum of colitis, we semi-quantitatively assessed the immune cell infiltration in different layers of the colon wall, graded tissue damage, and rated alterations in mucosal architecture as signs of tissue repair or neoplastic changes.

2. Materials and methods

In the following, we show the scoring results of three different models with a total of 129 mice. All samples were obtained from the Comparative Experimental Pathology (CEP) at the Institute of Pathology, Technical University of Munich (TUM), one of Europe's largest core facilities for comparative pathology.

Murine colitis models:

1. Metabolic injury induced by genetic deletion of the mitochondrial chaperone Hsp60, specifically in intestinal epithelial cells (IEC) ($Hsp60^{\Delta/\Delta IEC}$), causing MT-UPR (mitochondrial unfolded protein response) signaling and transient tissue injury in the murine intestine. This metabolic injury was defined as a cell-autonomous process of tissue wounding in response to mitochondrial perturbation (Rath and Haller, 2022). $Hsp60^{flox/flox}$ mice and $Hsp60^{flox/flox}$ x *Villin*-$CreER^{T2\text{-}Tg}$ mice (to generate IEC-specific Hsp60 knockout mice via tamoxifen induction ($Hsp60^{\Delta/\Delta IEC}$)) were generated as described previously (Berger et al., 2016). Gene deletion took place at 11 weeks of age, and mice were sacrificed 14 days later. A total of 24 male animals were examined (experimental group: $n = 12$; control group: $n = 12$).
2. Chemically induced colitis-associated cancer using Azoxymethane (AOM)/Dextran sodium sulfate (DSS), purchased from MP Biomedical (DSS colitis grade, MP Biomedical, molecular weight distribution 36,000–50,000 Da). Following the principles of the 3Rs (Replacement, Reduction, Refinement), we used samples of Bcl10-$^{flox/flox}$ mice with a C57BL/6 background, which did not undergo conditional knockout and served as control animals in another study.

   AOM/DSS treatment started at the age of 8 weeks and was carried out as follows: 10 mg/kg AOM was injected i.p. in 8 ml/kg physiological saline solution (day −5). On day 0 (5 days after AOM injection), the drinking water was replaced with water containing DSS (concentration: 2.6 %). After 5 days, the DSS water was replaced with normal drinking water. On days 21 to 25 (5 days), the drinking water was replaced with water containing DSS. This was repeated on days 42 to 46 (5 days). The experiment ended after 63 days or after reaching the humane endpoint. A total of 74 animals (male and female) were examined. 53 underwent AOM/DSS treatment, and 21 served as control animals.
3. Spontaneous enterocolitis in interleukin-10 (IL-10) deficient mice. Mice deficient in IL-10, an anti-inflammatory cytokine, develop spontaneous enterocolitis when housed under specific pathogen-free conditions. In contrast, IL-10−/− mice stay disease-free under germfree conditions (Sellon et al., 1998). The severity of the disease depends on several factors, including the genetic background (Mahler and Leiter, 2002). This study used C57BL/6 IL-10−/− mice and the respective wild-type (WT) mice. The mice were gavaged with two different modified versions of the Simplified Human Microbiota (SIHUMI) (Eun et al., 2014) consisting of the following seven bacterial strains: *Enterococcus faecalis* OG1RF, *Ruminococcus gnavus* ATCC 29149, *Bacteroides vulgatus* ATCC 8482, *Lactobacillus plantarum* WCFS1, *Bifidobacterium longum* subsp. *longum* ATCC 15707, *Fusobacterium nucleatum* subsp. nucleatum and either *Escherichia coli* NC101 (SIHUMI pks+) or the mutant strain *Escherichia coli* NC101 Δpks (SIHUMI Δpks). Both *Escherichia coli* strains were kindly provided by Christian Jobin's group (Arthur et al., 2012). The mice were gavaged once orally (at 4 weeks of age) and colonized for 12 weeks. A total of 31 animals (male and female) were analyzed (IL-10−/− − SIHUMI pks+: $n = 7$; IL-10−/− − SIHUMI Δpks: $n = 12$; WT - SIHUMI pks+: $n = 6$; WT - SIHUMI Δpks: $n = 6$).

For all three models, the experimental groups were age- and sex-matched with the control groups. No difference in phenotype was recognized between male and female animals. Mice of models 1 and 2 were housed under specific pathogen-free (SPF) conditions, and mice of model 3 under germfree conditions according to the criteria of the Federation for Laboratory Animal Science Associations (FELASA) (12 h light/dark cycles at 24–26 °C) in the mouse facilities at the Technical University of Munich (School of Life Sciences Weihenstephan and TranslaTUM, Center for Translational Cancer Research, Munich, Germany). All mice received a standard diet (autoclaved V1124–300, Ssniff) ad libitum and autoclaved water and were sacrificed by CO_2, isoflurane,

or cervical dislocation.

All animal experiments, maintenance, and breeding of mouse lines were approved by the Committee on Animal Health Care and Use of the state of Upper Bavaria (Regierung von Oberbayern; AZ ROB-55.2-2532.Vet_02–14-217, AZ ROB-55.2-2532.Vet_02–20-58, AZ ROB-55.2-2532.Vet_02–18-37, AZ ROB-55.2-2532.Vet_02–14-86, AZ ROB-55.2-2532.Vet_02–20-9, AZ ROB-55.2-1-54-2532-109-2015) and performed in strict compliance with the EEC recommendations for the care and use of laboratory animals (European Communities Council Directive of 24 November 1986 (86/609/EEC)).

To generate the histologic samples, the intestines were removed immediately after sacrifice and cleaned from stool. Colonic tissue was cut open and prepared as a "Swiss roll." Tissues were fixed in 4 % PBS-buffered formaldehyde, dehydrated, and embedded in paraffin (FFPE). For hematoxylin & eosin (H&E) staining, 2 to 4 µm sections were stained with hematoxylin (of Mayer) and 0.2 % eosin (ethanolic solution; both Medite, Burgdorf, Germany) in an automated staining machine (Leica, Soest, Germany). For periodic acid-Schiff / Alcian blue (PAS-AB) staining sections were stained manually with alcian blue (Fisher) for detection of acidic mucins (0.5 % *v*/v in 3 % acetic acid, pH = 2.5, 5 min) as well as periodic acid (0.5 % v/v, 10 min) co-stained with Schiff's reagent (Sigma-Aldrich) for neutral mucins (15 min). After laboratory processing, slides were scanned in 40× magnification using a whole-slide brightfield scanner (Aperio AT2, Leica Biosystems, Wetzlar, Germany; PreciPoint M8 microscope, Precipoint, Garching bei München, Germany) and displayed in the Aperio ImageScope 12.3 or Precipoint ViewPoint software. Colonic sections were then blindly assessed for immune cell infiltration, epithelial damage, and alterations in mucosal architecture. The grading system described below resulted in a score from 0 (no inflammation) to 12 (severe inflammation).

We initially developed the scoring scheme using an IBD mouse model covering the entire disease spectrum, including tumorigenesis. Subsequently, we validated the scoring scheme in three additional mouse models.

Finally, a PhD student in veterinary medicine and a resident in veterinary pathology with broad experience in intestinal mouse pathology carried out a second assessment. Statistical analysis was performed with IBM SPSS Statistics (1200) 29.0 and GraphPad Prism 5. For comparison between two groups, Student's two-tailed unpaired *t*-test was used. Interrater variability was tested using Pearson's correlation. $P < 0.05$ was considered significant. $^{*}p<0.05$; $^{**}p<0.01$; $^{***}p<0.001$; $^{****}p<0.0001$. Data is presented as mean ± SD.

3. Results

3.1. Criteria for the histopathological evaluation of murine IBD models

We defined immune cell infiltration, mucosal damage, and changes in mucosal architecture as the three main categories correlating with inflammation. These categories were determined by 12 subordinate criteria (Fig. 1). Since inflammation often shows a patchy pattern, inflammatory hotspots were chosen for the analysis.

Leucocyte infiltration is the most prominent histological feature of inflammatory processes, and therefore, 6 of 12 score values were given to the immune cell infiltrate in different wall layers. The analysis was performed in a semi-quantitative manner. The infiltration by different types of leucocytes (e.g., lymphocytes, macrophages, neutrophils, mast cells) was not considered. Since leucocyte infiltration is generally most prominent in the mucosal lamina propria and spreads to deeper layers only in cases of severe inflammation, we assigned a maximum score of 3 to the immune cell infiltrate in the lamina propria (0 = no infiltrate, 1 = mild infiltrate, 2 = moderate infiltrate, 3 = severe infiltrate), 2 to the submucosa (0 = no infiltrate, 1 = mild to moderate infiltrate, 2 = severe infiltrate) and 1 to the muscularis (0 = no to mild infiltrate, 1 = moderate to severe infiltrate) (Fig. 2). A similar rating system has first been described by Katakura et al. (2005). Since few leucocytes are always detectable in the mucosa of non-germ-free mice, a score of 0 for immune cell infiltrate can only be expected in germ-free or leucocyte-depleted mice, whereas a normal and healthy colon will most likely reach a score of 1 or 2.

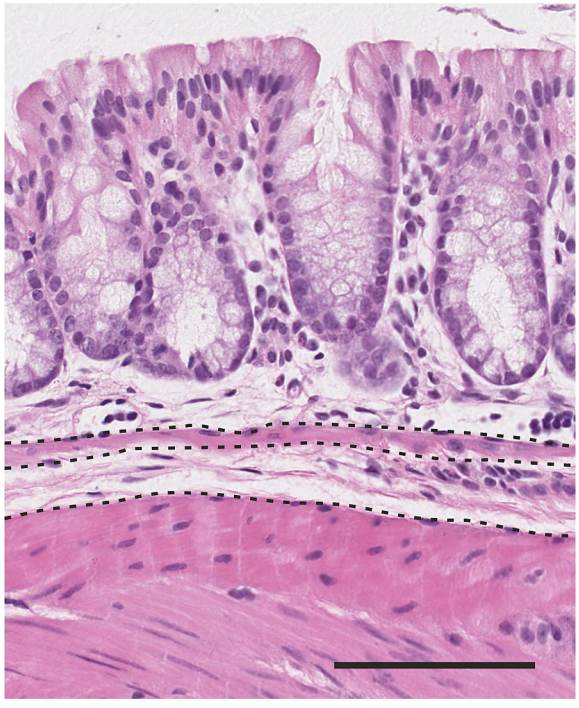

Immune cell infiltrate	
Mucosa - normal	0
Mucosa - mild	1
Mucosa - modest	2
Mucosa - severe	3
Submucosa - normal	0
Submucosa - mild to modest	1
Submucosa - severe	2
Muscularis – normal	0
Muscularis - moderate to severe	1
Epithelial damage	
No change	0
Epithelial infiltrate	1
Crypt abscesses, erosion	2
Ulcerations	3
Mucosal architecture/atypia	
No change	0
Simple hyperplasia without dysplasia	1
Low- and high-grade dysplasia	2
Invasive carcinoma	3
Max. Score	**12**

Fig. 1. Evaluation criteria. A representative cross-section of the inflammation-free colon wall in a control animal of model 1 (Score 0, H&*E*-staining) on the left. The dashed lines mark the interfaces between individual wall layers. Scale bar: 100 µm. The table on the right shows an overview of the categories and scores to be applied to the colitis score presented here. The total score can range from 0 (no inflammation) to 12 (severe acute and chronic inflammation with formation of an invasive carcinoma).

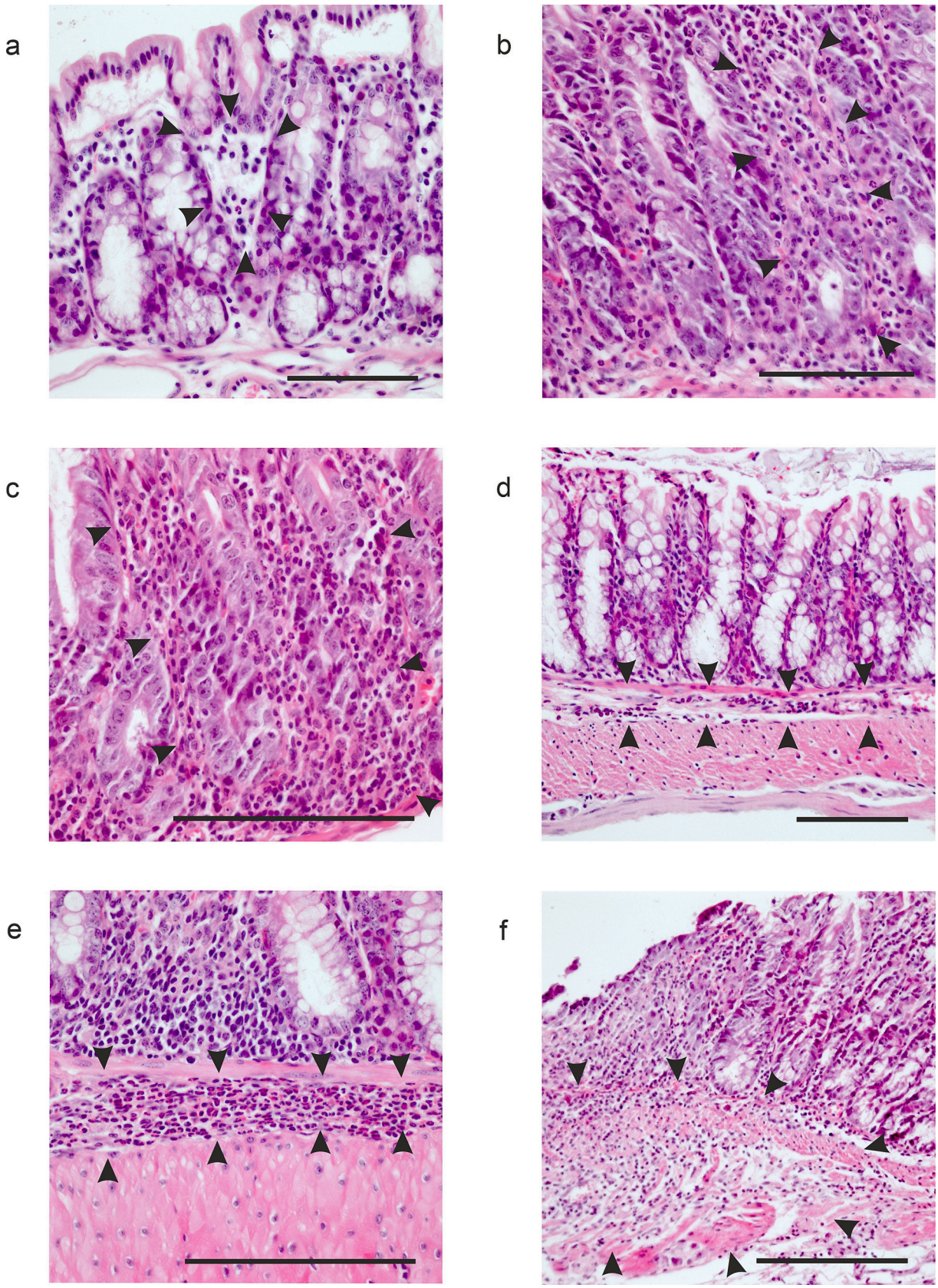

Fig. 2. Immune cell infiltrate. (a) Mild mucosal immune cell infiltrate (1 point in the colitis score); (b) Moderate mucosal immune cell infiltrate (2 points in the colitis score); (c) Severe mucosal immune cell infiltrate (3 points in the colitis score); (d) Mild to moderate submucosal immune cell infiltrate (1 point in the colitis score); (e) Severe submucosal immune cell infiltrate (2 points in the colitis score); (f) Immune cell infiltrate in muscularis propria (1 point in the colitis score). The arrowheads mark the relevant immune cell infiltrate in the respective anatomical sites (mucosa, submucosa, muscularis). (a) shows a representative image of control animals in model 1, (b-f) show representative H&E stainings of AOM/DSS-treated animals in model 2. Scale bars: 100 μm.

The second hallmark of inflammation is tissue damage. Epithelial damage due to inflammation was graded into 4 categories from 0 (no epithelial damage) to 3. Enhancement of intraepithelial lymphocytes (IELs) is graded as 1 (mild epithelial damage), erosions and crypt abscesses are graded as 2 (moderate epithelial damage), and a score of 3 (severe epithelial damage) is accredited to ulcerations (Fig. 3). Healthy colonic mucosa should have no ulcerations, erosions, crypt abscesses, or increased IELs and is therefore assigned a score of 0 (Fig. 1). The main histomorphological characteristics of erosions, ulcerations, IELs, and crypt abscesses are listed in Table 1.

Since chronic inflammation and tumorigenesis have a strong functional relationship (Kappelman et al., 2014), we also screened for changes in mucosal architecture, which were graded in 4 categories. Colonic mucosa without architectural changes was rated 0. A value of 1 corresponds to simple hyperplasia without dysplasia as a correlate of increased tissue turn-around and tissue repair, whereas the values 2 (low- and high-grade dysplasia) and 3 (invasive carcinoma) correspond to neoplastic lesions (Fig. 4).

Simple hyperplasia is defined by the thickening of the mucosa with elongated crypts without dilation, mild nuclear enlargement without significant stratification, or hyperchromasia of nuclei. Goblet cells are rare. Low-grade dysplasia, however, is characterized by hyperchromatic, often elongated nuclei and nuclear stratification. Goblet cells are depleted. High-grade dysplasia additionally shows loss of cell polarity, complex glandular crowding, and cribriform architecture. An adenocarcinoma in the colon of rodents is, according to the International Harmonization of Nomenclature and Diagnostic (INHAND) Criteria of the Society of Toxicologic Pathology, defined by the spread of neoplastic cells outside the lamina muscularis mucosae (Nolte et al., 2016) (Table 1, Fig. 5).

3.2. Pitfalls in the evaluation of IBD mouse models

We are aware of some critical pitfalls in the histological assessment of colitis models. The most crucial point is distinguishing between immune cell infiltrates and regular lymphoid follicles / Peyer's patches. Peyer's patches are collections of lymphoid follicles in the mucosa of the small intestine but are also frequently observed in the caecum, especially in inflammatory bowel conditions. They are generally more frequent in mice than in the human intestine, where they are typically found in the terminal ileum. If these Peyer's patches are cut centrally, they can be easily recognized. However, if only the edge is visible on the histological slide, Peyer's patches can be mistaken for inflammatory infiltrates of the mucosa or submucosa. In contrast to purely inflammatory infiltrates, Peyer's patches have follicle-associated surface epithelium and quite monomorphic lymphocyte aggregates (Fig. 6a-c).

One should be aware that to obtain a reliable evaluation, immune cells in connective tissue along vessels penetrating the muscularis propria should not be graded as infiltration of muscularis propria (Fig. 6d). Additionally, simple mucosa folds can be misinterpreted as tumors. Another reason for the misdiagnosis of invasive carcinoma is mucosal invaginations, i.e., protrusions of the intestinal mucosa through the lamina propria into the submucosa. However, specific histological criteria of the surface epithelium must be fulfilled to diagnose a malignant neoplasia. These include increased basophilia, a nucleus-plasma ratio shifted in favor of the nucleus, and architectural irregularities (Fig. 6e, f).

Artefacts might arise if the tissue is poorly fixed. Autolytically damaged surface cells appear as small cells with dense chromatin and no discernible cytoplasmic border and can easily be mistaken for infiltrating lymphocytes. Poor fixation reduces the diagnostic certainty because defining the cell type and analyzing the tissue architecture can only be assessed to a limited extent. Sampling errors are another reason for inaccurate results. Especially if the inflammation is patchy and evaluation is done in hotspots, there is a considerable risk of incorrectly low scores if only small tissue samples instead of whole Swiss rolls are submitted.

Since many strains and stocks of mice, including C57BL/6 mice, develop lymphomas as a background lesion, especially seen in aging mice, lymphomas should be considered as a differential diagnosis. The possibility of lymphoma must especially be considered if there is a striking monomorphic lymphocytic infiltrate that respects the architecture of the colon and other histomorphological features of colitis are absent. Differentiating reactive inflammation from lymphoma can be challenging (Ward et al., 2006; Ward et al., 2012). In doubtful cases, immunohistochemical staining for B-cells (e.g., CD20) and T-cells (e.g., CD3) helps to differentiate between inflammation and lymphoma, as reactive lymphocytic infiltrates always show a mixed inflammatory infiltrate (B- and T-cells). In contrast, one cell type dominates in lymphomas depending on the cell of origin (Ward, 2006). If a lymphoma is suspected, examining the other organs for lymphoma-typical changes like enlarged lymph nodes or hepatosplenomegaly is also helpful.

3.3. Results from different models

To validate our colitis score, we used three different mouse models covering the whole spectrum of inflammatory bowel disease (from acute and transient inflammation to chronic inflammation, including tumorigenesis as a late sequela of IBD). All three colitis models showed clear and significant discrimination between experimental and control groups (Fig. 7). Images of representative hotspots of all three models are provided as supplementary material (Supplementary figures S1-S3).

In model 1 (genetic model developing metabolic injury), the experimental group ($Hsp60^{\Delta/\Delta IEC}$) reached an average score of 5.42 ± 0.96 ($n = 12$) and hence differed significantly ($p < 0.0001$) from the control group with an average score of 0.83 ± 0.37 ($n = 12$) (Fig. 7a).

The chemically induced model (model 2) also showed a significantly higher score ($p < 0.0001$) in the AOM/DSS-treated group (7.02 ± 1.81, $n = 53$) than in the control group (1.29 ± 0.63, $n = 21$) (Fig. 7b).

In model 3 (spontaneous colitis in IL10-deficient mice), we compared IL-10 deficient mice colonized with the Simplified Human Microbiota (SIHUMI) containing *E. coli* NC101 ($IL\text{-}10^{-/-}$ − SIHUMI pks+) and IL-10 deficient mice colonized with the Simplified Human Microbiota containing *E. coli* NC101 Δpks ($IL\text{-}10^{-/-}$ − SIHUMI Δpks) to corresponding wild type animals (WT - SIHUMI pks + or WT - SIHUMI Δpks). We could show a significant difference between IL-10-deficient and wild-type mice for both versions of the Simplified Human Microbiota. In the SIHUMI pks + −setting, IL10-deficient mice had an average score of 2.13 ± 1.12 ($n = 7$), whereas wild-type mice showed an average score of 1.00 ± 0.00 ($n = 6$) ($p = 0.047$). In the SIHUMI Δpks-setting IL10-deficient mice reached an average score of 4.25 ± 2.01 ($n = 12$), and wild-type mice reached an average score of 1.00 ± 0.00 ($n = 6$) ($p < 0.001$). The comparison of $IL\text{-}10^{-/-}$ − SIHUMI pks + vs. $IL\text{-}10^{-/-}$ − SIHUMI Δpks proves the discriminatory power of our score. The differences in the microbiome alone resulted in a significantly different score ($p = 0.013$) (Fig. 7c).

3.4. Interrater reliability

To test for interrater reliability, 80 samples from different models and all degrees of inflammation were evaluated independently by an experienced human pathologist and an experienced veterinary pathologist. The results of both raters showed a strong correlation, $r = 0.888$, $p < 0.0001$ (Fig. 8a, c).

Since we aimed to develop a scoring scheme that is also suitable for researchers without a profound pathological background, the same samples were assessed by a PhD student in veterinary medicine. The results also showed a strong correlation, $r = 0.780$, $p < 0.001$ (Fig. 8b, c).

4. Discussion

Histomorphological grading is a powerful, easy, and cost-efficient

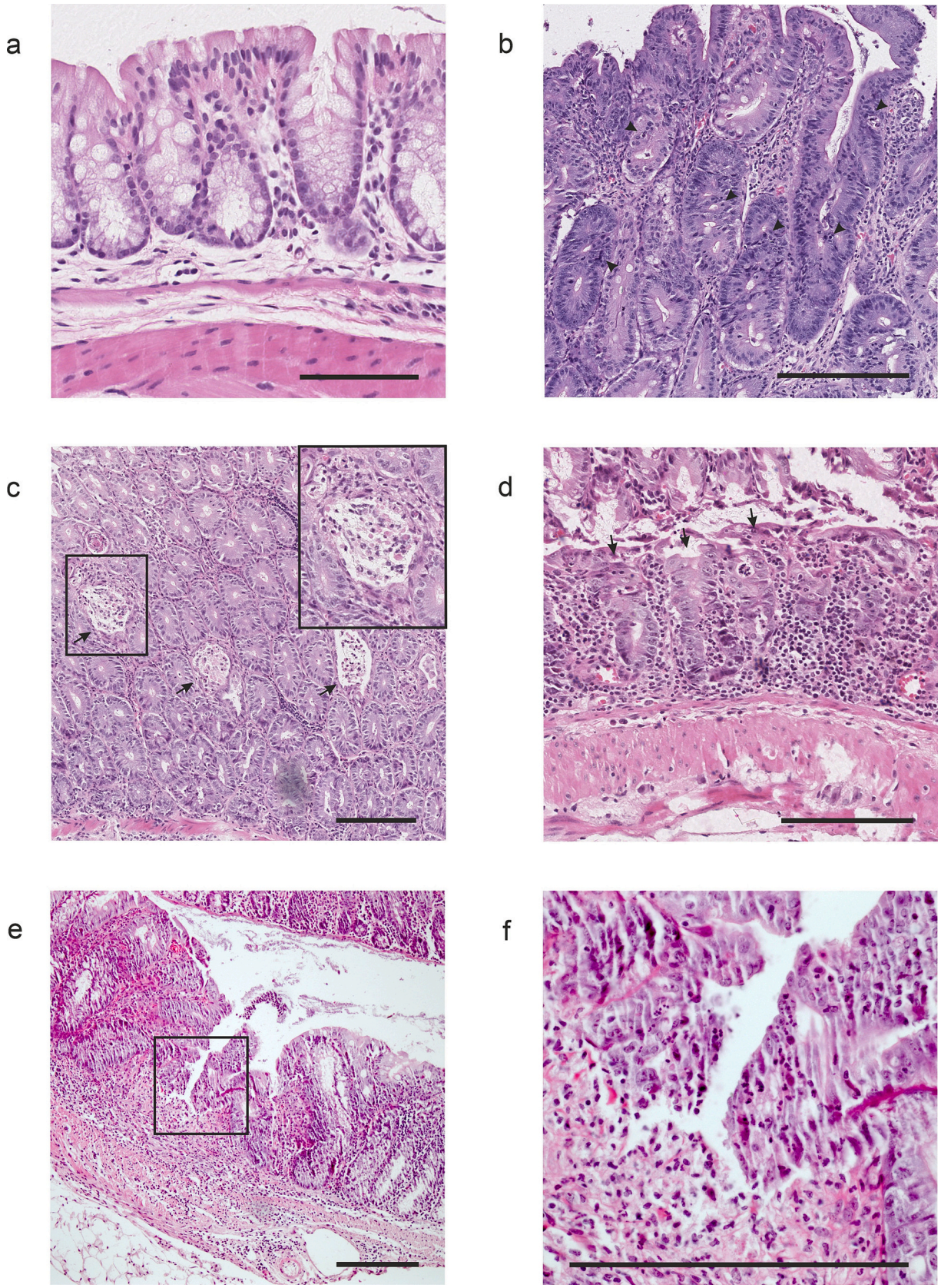

Fig. 3. Epithelial damage. (a) Colon mucosa without significant epithelial damage; (b) Increased intraepithelial leucocytes (arrowheads) representing the mildest form of epithelial damage (1 point in the colitis score); (c) Crypt abscesses (arrows) and (d) erosion (arrows) of surface epithelium as a correlate of moderate epithelial damage (2 points in the colitis score); (e, f) Ulcerations as the maximum variant of epithelial damage (3 points in the colitis score, f corresponds to the insert in e). (a) shows a representative H&E staining of control animals in model 1, (b, c) show representative H&E stainings of animals with metabolic injury in model 1, (d-f) show representative H&E stainings of AOM/DSS-treated animals in model 2. Scale bars: 100 μm.

Table 1
Nomenclature of inflammatory tissue changes with description of essential histomorphological characteristics.

	Nomenclature	Histomorphological characteristics	Points in colitis score
Epithelial damage	Intraepithelial lymphocytes (Fig. 3b)	• Lymphocytes (small round cells without discernible cytoplasm) located between epithelial cells of the intestinal mucosa.	1
	Crypt abscesses (Fig. 3c)	• Masses of neutrophile granulocytes (immune cells with typically segmented nuclei) accumulating in a crypt lumen. • Loss of the epithelium, intact basement membrane.	2
	Erosion (Fig. 3d)	• Fibrin depositions and inflammatory cell infiltrate distinguish true, intravital-developed erosions from artificial epithelial denudation due to aggressive tissue handling. • Loss of epithelium in a localized area.	2
	Ulceration (Fig. 3e, f)	• Extends beyond the basement membrane into deeper tissue layers.	3
Architectural alterations	Hyperplasia (Fig. 4b)	• Often widespread and broad-based thickening of the mucosa. • Preserved polarity: The cell nuclei are located basally (above the basement membrane), apical cytoplasmic cap. • Nuclei are enlarged but monomorphic and without significant atypia (no pronounced nuclear size variations, chromatin regularly distributed, no increased staining of the nuclei). • Mitoses (as a sign of increased proliferative activity) are limited to the crypt bases (stem cell niche). • Nuclei of the epithelial cells enlarged, elongated, and with increased staining intensity (hyperchromasia).	1
	Low-grade dysplasia (Fig. 4c, d; Fig. 5a, b, d)	• Palisade-like arrangement of the nuclei. • Increased mitoses, also ascending (outside the crypt bases). • Reduced mucin production (no / only very small goblet cells). • Crypts are elongated and without irregular branching. • See low-grade dysplasia.	2
	High-grade dysplasia (Fig. 4e, f; Fig. 5e)	Additionally: • Irregularly branching crypts. • Stronger cytological atypia (enlarged hyperchromatic nuclei with prominent nucleoli, numerous mitoses, occasional necrosis).	2
	Invasive adenocarcinoma (Fig. 4e, f; Fig. 5f)	• Same cytological features as high-grade dysplasia. • Invasive growth, defined by the spread of neoplastic cells below the lamina muscularis mucosae. • Invasive cell nests are often surrounded by dense connective tissue (desmoplastic stroma).	3

tool for evaluating murine colitis and colitis-associated cancer models. However, many research groups do not take advantage of histomorphology due to the lack of expertise and due to the lack of (veterinary) pathologists with knowledge in comparative medicine (Steiger et al., 2019). To our knowledge, there is not yet an established colitis score that can be applied to different models, enabling a comparison of different models concerning inflammatory activity.

In this study, we established an easy and reliable method to score different murine IBD models. We developed a scoring system that covers all disease stages and phenotypes, from purely inflammatory changes to tumorigenesis, allowing the comparison of different models regarding inflammatory activity and inflammation-related lesions.

Many previously described scoring models were developed for one specific mouse model, and the examined criteria often cannot be transferred to all IBD models. Erben et al. (2014) created a systematic overview of different damage patterns in the colon with corresponding scoring schemes, allowing a differentiated evaluation of IBD models. However, the associated complexity requires a high level of expertise in intestinal histopathology on the part of the diagnostician, which is unfortunately not readily available in many institutes. The use of different scores for different triggers of intestinal inflammation with different maximum score values makes it difficult to compare individual models. Additionally, neoplastic lesions are not included in scoring schemes established by Erben et al. (2014).

Collaboration with non-pathologists has shown that simple and universal evaluation criteria are needed, which can be reproduced and applied by non-pathologists, too. Hence, we reduced the score to well-recognizable features representing different stages of the disease (acute colitis and colitis-associated tumorigenesis) and a simple, semi-quantitative analysis of the immune cell infiltrate as a measure of inflammation severity. The semi-quantitative analysis allows the transformation of qualitative tissue data into numerical data for more robust group comparisons. In contrast to quantitative tools, semi-quantitative analysis is more reproducible and is more time-efficient (Meyerholz and Beck, 2018).

As we intentionally developed a score that is as general as possible to cover various mouse models and disease stages, the score may not differentiate well between experimental groups that differ only slightly in their phenotype. In these cases, it is useful to complement the score with additional parameters. Parameters that have proven useful include the percentage of tissue with the highest colitis score, the percentage of tissue without significant inflammation (score 0–2), separate scores for different colon segments (e.g., oral, middle, aboral), or the number of detected tumors. Also, our score could lose some of its precision by not accurately characterizing the type of inflammation. However, recognizing different types of inflammatory cells or types of inflammation (acute, chronic, granulomatous, etc.) is challenging for non-pathologists and is associated with a high inter-rater variability. Some cell types, such

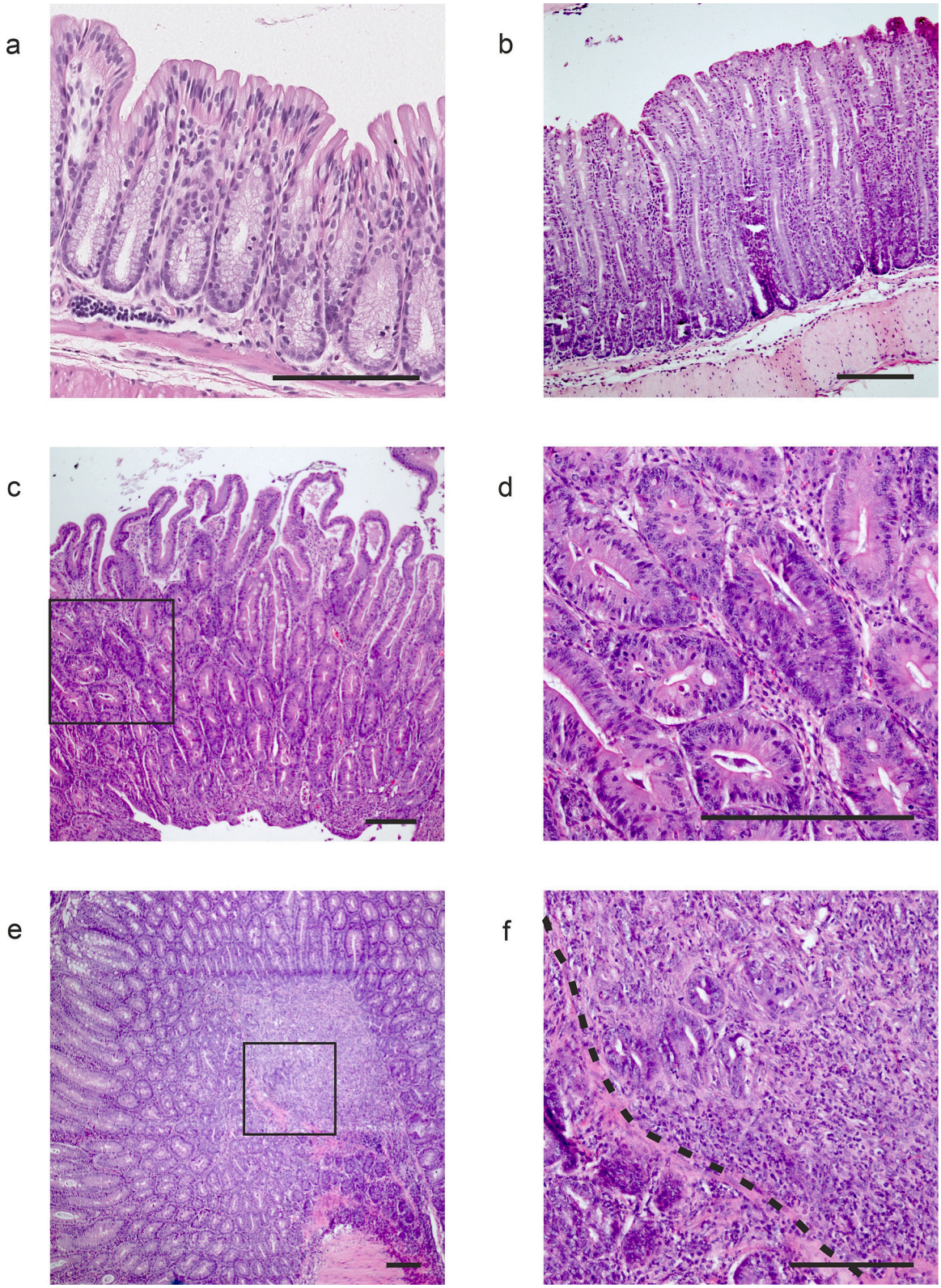

Fig. 4. Architectural aberrations. (a) Architecturally regular colorectal mucosa without dysplasia (0 points in the colitis score); (b) Simple hyperplasia without dysplasia (1 point in the colitis score); (c, d) Colorectal adenoma with low-grade intraepithelial neoplasia/dysplasia (2 points in the colitis score, d corresponds to the insert in c); (e, f) Colorectal adenoma with high-grade intraepithelial neoplasia/dysplasia and focal transition to invasive growth (see insert in e; f). The findings, therefore, correspond to an invasive adenocarcinoma (3 points in the colitis score). The dashed line in f represents the lamina muscularis mucosae. (a) Shows a representative H&E staining of control animals in model 1, (b) shows a representative H&E staining of IL $10^{-/-}$ SIHUMI Δ-pks animals in model 3, (c-f) show representative H&E stainings of AOM/DSS-treated animals in model 2. Scale bars: 100 μm.

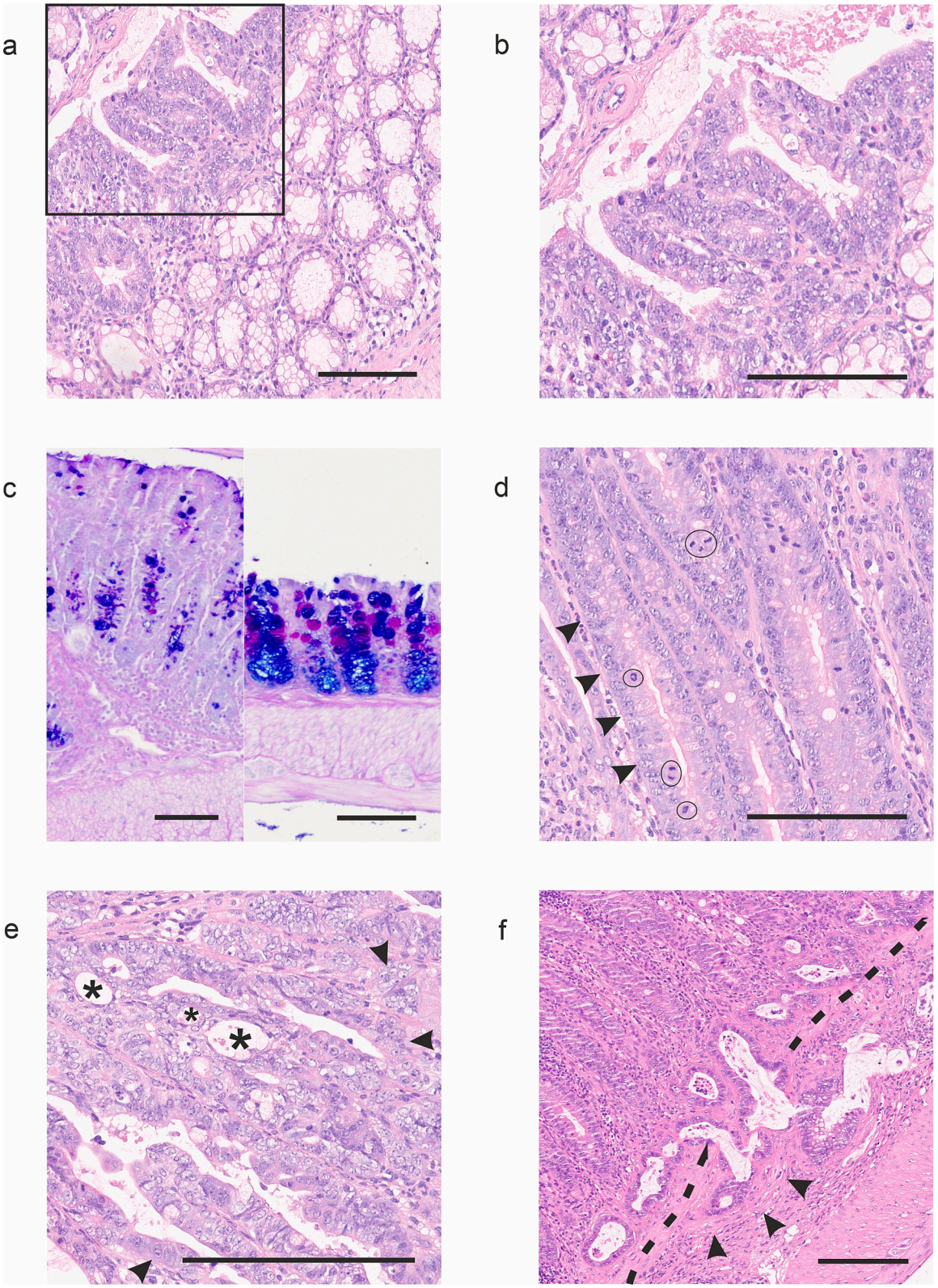

Fig. 5. Mucosal architecture and neoplastic changes. (a) Regular colonic mucosa (bottom right) with transition to low-grade dysplasia (top left); (b) corresponds to the insert in a. Note the increased basophilia in low-grade dysplasia due to enlarged, hyperchromatic nuclei and loss of goblet cells; (c) Loss of goblet cells in low-grade dysplasia (left) compared to regular colonic mucosa (right), highlighted by PAS-AB staining; (d) Increased mitoses (circles) and palisade like arrangement of nuclei (arrowheads) in low-grade dysplasia; (e) Crowded, enlarged and pleomorphic nuclei with prominent nucleoli (arrowheads), loss of cell polarity and complex architecture with poorly formed crypts and cribriform architecture with formation of secondary lumina (asterisks) in high-grade dysplasia; (f) Invasive carcinoma with penetration of the lamina muscularis mucosae (dashed line) and spread of neoplastic glands in the submucosa. The neoplastic glands in the submucosa are surrounded by desmoplastic stroma (arrowheads). All images show representative H&E (a, b, d-f) or PAS-AB (c) stainings of AOM/DSS-treated animals in model 2. Scale bars: 100 μm.

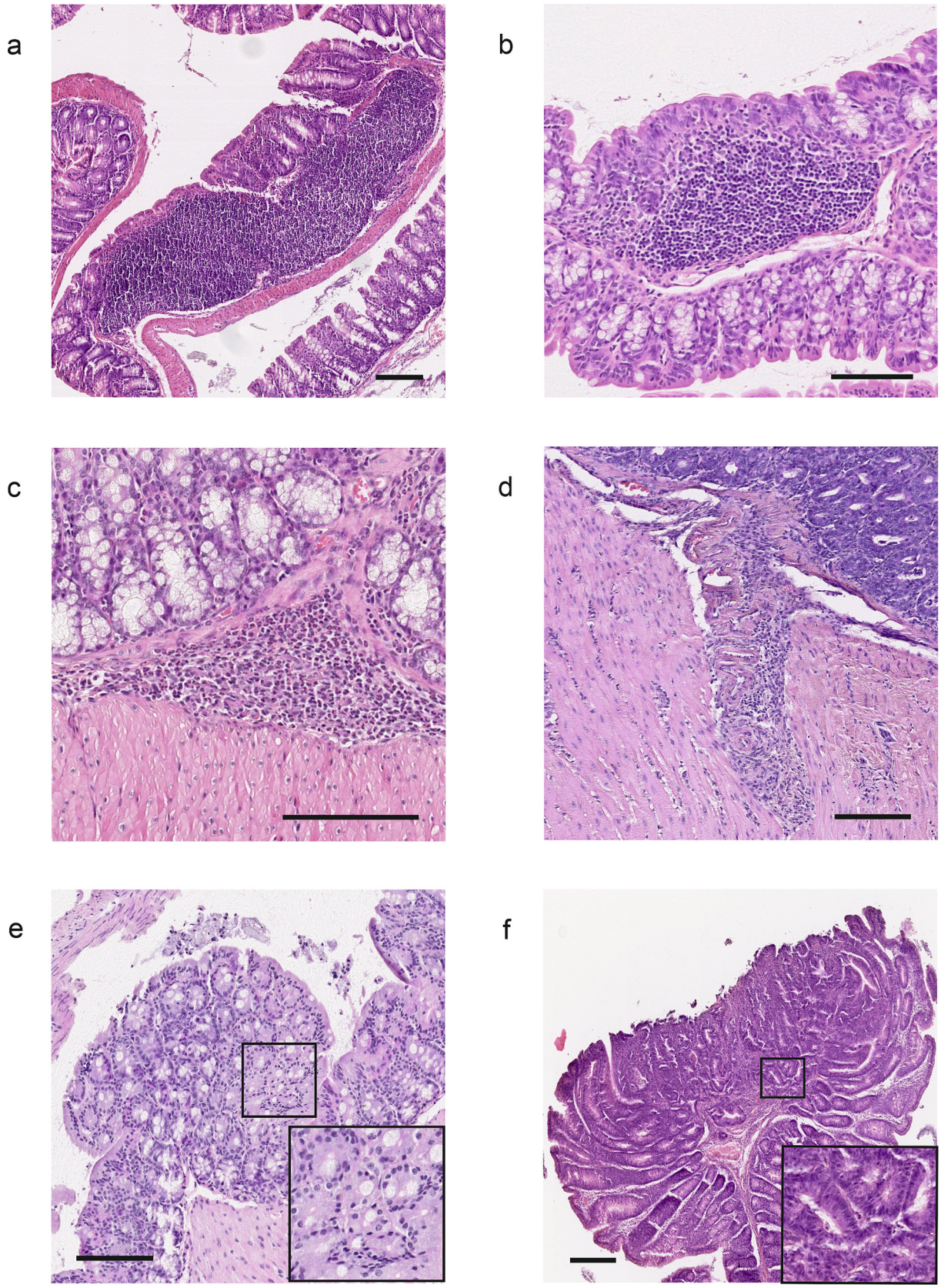

Fig. 6. Pitfalls. (a) Big, centrally recorded Peyer's patch; (b) Smaller, marginally recorded Peyer's patch; (c) Inflammatory infiltrate; (d) Immune cell infiltrate along connective tissue and vessels penetrating the muscularis propria; (e) Simple mucosa fold without dysplasia; (f) Adenoma with high-grade dysplasia. (a, b) show representative H&E stainings of control animals in model 3, (c, d) show representative H&E stainings of IL $10^{-/-}$ SIHUMI Δ-pks animals in model 3, (e, f) show representative H&E stainings of AOM/DSS-treated animals in model 2. Scale bars: 100 μm.

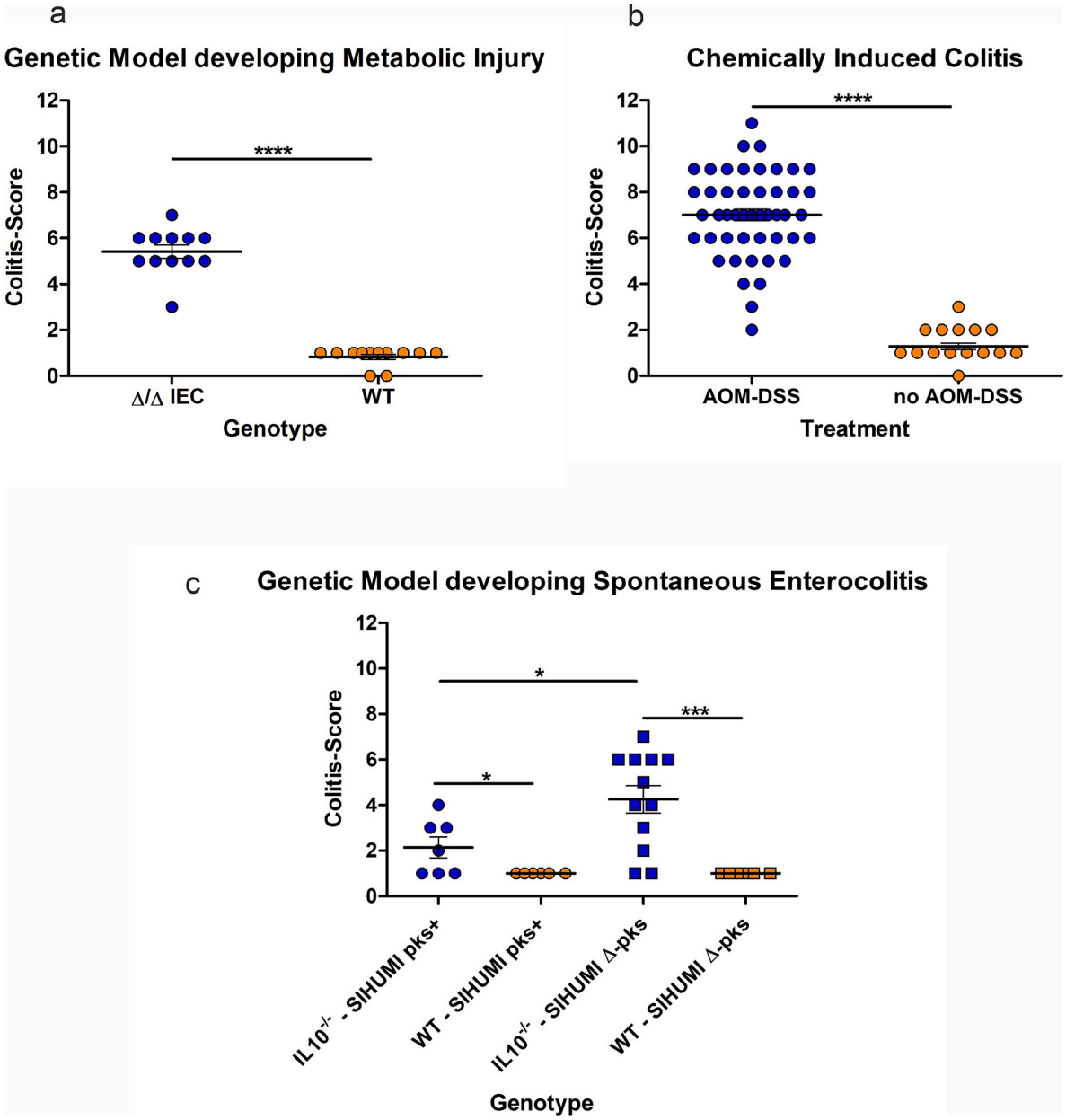

Fig. 7. Validation of our colitis score using three different mouse models. Model 1 (a): Colitis score is significantly higher in mice suffering from metabolic injury ($n = 12$) than in littermates without metabolic injury ($n = 12$). Model 2 (b): Treatment with AOM/DSS results in a 5-fold higher score ($n = 53$) compared to untreated controls ($n = 21$). Model 3 (c): IL10-deficient mice score significantly higher than wild-type mice colonized with the same microbiota. Our colitis score also shows significant differences in IL-10 deficient mice colonized with different microbiota (IL $10^{-/-}$ SIHUMI pks + vs. IL $10^{-/-}$ SIHUMI Δ-pks). *P*-values were calculated by *t*-test: $^{*}p < 0.05$, $^{**}p < 0.01$, $^{***}p < 0.001$, $^{****}p < 0.0001$. IL-$10^{-/-}$ − SIHUMI pks+: $n = 7$; WT SIHUMI pks+: $n = 6$; IL-$10^{-/-}$ − SIHUMI Δpks: $n = 12$; WT SIHUMI Δpks: $n = 6$.

as mast cells, can only be reliably assessed with special stains (toluidine blue or Giemsa) or immunohistochemistry (Groll et al., 2022). In addition, the type of inflammation within a model is usually uniform, so precise classification can be neglected in inflammation scoring. However, the exact description of the inflammatory processes should still be carried out by an experienced pathologist as part of the characterization of new models.

If a measure of the type of inflammation or disease activity is required, the score may be complemented by computer-assisted methods for quantifying neutrophil granulocytes or other cell types. Various open-source and commercially available software suits this purpose (Bankhead et al., 2017).

To make scoring technically as simple as possible, we have also decided not to use additional stains like Alcian blue - periodic acid–Schiff (AB-PAS) staining for the visualization of goblet cells, as we are convinced that goblet cells can also be assessed on H&E staining with sufficient certainty. In the training phase, however, PAS-AB staining could facilitate the detection of relevant lesions.

The score presented here has already been successfully used by Urbauer et al. (2024). We could show that the score differentiates well between the individual experimental groups in highly complex mouse models, correlates with the results of molecular investigations (e.g., level of Trb3-mRNA as a correlate of mitochondrial unfolded protein response and cellular stress response), and reproduces the temporal course of inflammation. Furthermore, the score showed reliable significance not only in the colon but also in samples taken from the ileum,

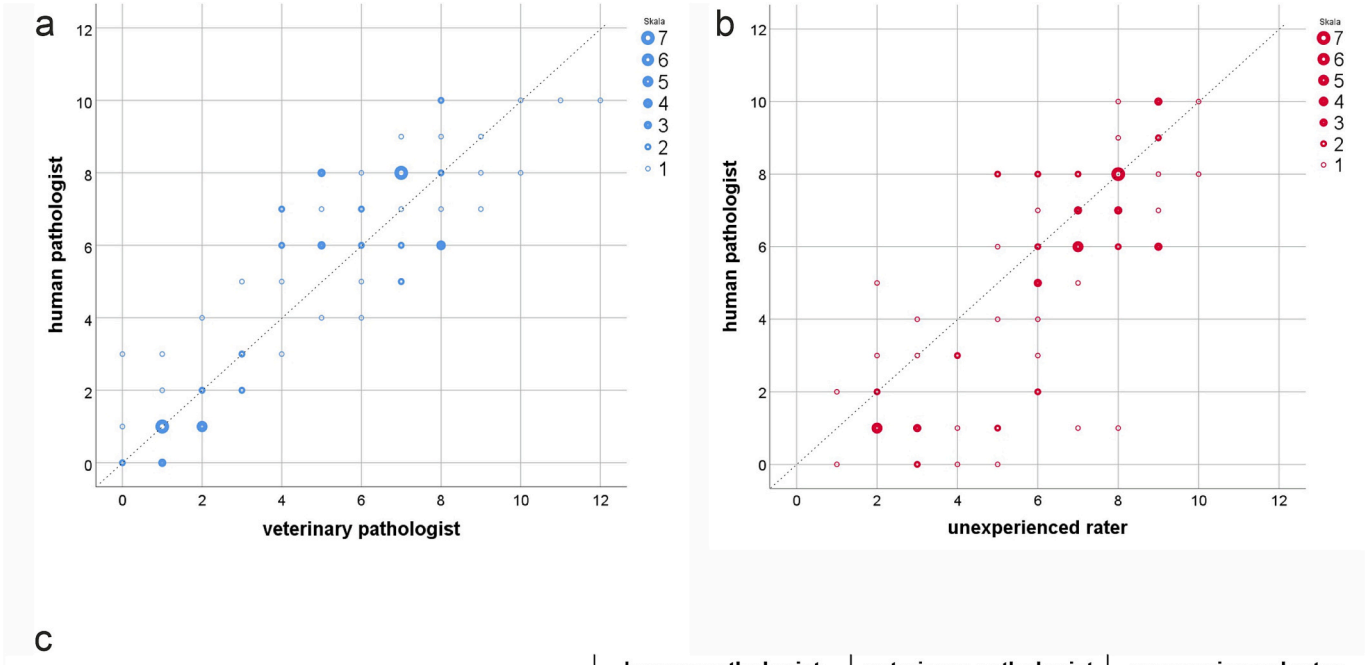

c

		human pathologist	veterinary pathologist	unexperienced rater
human pathologist	Pearson-Correlation	1	0.888	0.780
	Significance (2-sided)		<0.0001	<0.0001
	N	80	80	80
veterinary pathologist	Pearson-Correlation	0.888	1	0.739
	Significance (2-sided)	<0.0001		<0.0001
	N	80	80	80
unexperienced rater	Pearson-Correlation	0.780	0.739	1
	Significance (2-sided)	<0.0001	<0.0001	
	N	80	80	80

Fig. 8. Interrater reliability. (a) Score correlation between a human pathologist and a veterinary pathologist; (b) Results correlation between a human pathologist and an unexperienced rater; (c) Statistical evaluation (Pearson correlation), $n = 80$.

highlighting its wide range of applicability.

Our results showed that the score allows a reliable assessment of different murine IBD models and provides reproducible results. The application of this score can be learned with little experience in histomorphology. The detailed histological illustrations included in this work are intended to further facilitate this. Nevertheless, training and the occasional discussion of findings by (veterinary) pathologists with experience in murine IBD models are recommended. After training, however, scientists can perform the scoring themselves under the supervision of a pathologist, thus saving the limited personnel resources of pathologists with experience in lab animal pathology. As a result, histomorphology can gain importance as a cost-effective and reliable analytical tool. We hope that this score will make the histomorphological assessment of IBD models accessible to more research groups and helps histopathology regain its deserved status alongside the new molecular methods.

5. Conclusion

The scoring scheme we developed is easy to learn and reproducible, and it discriminates well between different stages of inflammation. It enables researchers to benefit from histomorphology as a cost-effective and reliable tool in analyzing all kinds of murine IBD models.

Supplementary data to this article can be found online at https://doi.org/10.1016/j.yexmp.2024.104938.

Funding

This work was supported by the Deutsche Forschungsgemeinschaft (DFG, German Research Foundation) Collaborative Research Center CRC 1371 (Microbiome signatures: functional relevance in the digestive tract; project no. 395357507; Z01).

CRediT authorship contribution statement

Marianne Remke: Writing – original draft, Methodology, Formal analysis, Data curation, Conceptualization. **Tanja Groll:** Writing – review & editing, Validation. **Thomas Metzler:** Validation. **Elisabeth Urbauer:** Resources, Methodology. **Janine Kövilein:** Resources, Methodology. **Theresa Schnalzger:** Resources, Methodology. **Jürgen Ruland:** Resources, Methodology. **Dirk Haller:** Resources, Methodology. **Katja Steiger:** Writing – review & editing, Supervision, Resources, Methodology, Conceptualization.

Declaration of generative AI and AI-assisted technologies in the writing process

During the preparation of this work, the authors used DeepL Write to improve the manuscript's readability and language. After using this tool/service, the author(s) reviewed and edited the content as needed and take full responsibility for the content of the published article.

Declaration of competing interest

All authors declare no conflicts of interest related to this work.

Data availability

Data will be made available on request.

References

Arthur, J.C., Perez-Chanona, E., Muhlbauer, M., Tomkovich, S., Uronis, J.M., Fan, T.J., Campbell, B.J., Abujamel, T., Dogan, B., Rogers, A.B., Rhodes, J.M., Stintzi, A., Simpson, K.W., Hansen, J.J., Keku, T.O., Fodor, A.A., Jobin, C., 2012. Intestinal inflammation targets cancer-inducing activity of the microbiota. Science 338 (6103), 120–123. https://doi.org/10.1126/science.1224820.

Bankhead, P., Loughrey, M.B., Fernandez, J.A., Dombrowski, Y., McArt, D.G., Dunne, P. D., McQuaid, S., Gray, R.T., Murray, L.J., Coleman, H.G., James, J.A., Salto-Tellez, M., Hamilton, P.W., 2017. QuPath: open source software for digital pathology image analysis. Sci. Rep. 7 (1), 16878. https://doi.org/10.1038/s41598-017-17204-5.

Baydi, Z., Limami, Y., Khalki, L., Zaid, N., Naya, A., Mtairag, E.M., Oudghiri, M., Zaid, Y., 2021. An update of research animal models of Inflammatory Bowel Disease. ScientificWorldJournal 2021, 7479540. https://doi.org/10.1155/2021/7479540.

Berger, E., Rath, E., Yuan, D., Waldschmitt, N., Khaloian, S., Allgauer, M., Staszewski, O., Lobner, E.M., Schottl, T., Giesbertz, P., Coleman, O.I., Prinz, M., Weber, A., Gerhard, M., Klingenspor, M., Janssen, K.P., Heikenwalder, M., Haller, D., 2016. Mitochondrial function controls intestinal epithelial stemness and proliferation. Nat. Commun. 7, 13171. https://doi.org/10.1038/ncomms13171.

Charlebois, A., Rosenfeld, G., Bressler, B., 2016. The impact of dietary interventions on the symptoms of inflammatory Bowel disease: a systematic review. Crit. Rev. Food Sci. Nutr. 56 (8), 1370–1378. https://doi.org/10.1080/10408398.2012.760515.

Cheng, J.Y., Abel, J.T., Balis, U.G.J., McClintock, D.S., Pantanowitz, L., 2021. Challenges in the development, deployment, and regulation of artificial intelligence in anatomic pathology. Am. J. Pathol. 191 (10), 1684–1692. https://doi.org/10.1016/j.ajpath.2020.10.018.

Chu, H., Khosravi, A., Kusumawardhani, I.P., Kwon, A.H., Vasconcelos, A.C., Cunha, L. D., Mayer, A.E., Shen, Y., Wu, W.L., Kambal, A., Targan, S.R., Xavier, R.J., Ernst, P. B., Green, D.R., McGovern, D.P., Virgin, H.W., Mazmanian, S.K., 2016. Gene-microbiota interactions contribute to the pathogenesis of inflammatory bowel disease. Science 352 (6289), 1116–1120. https://doi.org/10.1126/science.aad9948.

Erben, U., Loddenkemper, C., Doerfel, K., Spieckermann, S., Haller, D., Heimesaat, M.M., Zeitz, M., Siegmund, B., Kuhl, A.A., 2014. A guide to histomorphological evaluation of intestinal inflammation in mouse models. Int. J. Clin. Exp. Pathol. 7 (8), 4557–4576. https://www.ncbi.nlm.nih.gov/pubmed/25197329.

Eun, C.S., Mishima, Y., Wohlgemuth, S., Liu, B., Bower, M., Carroll, I.M., Sartor, R.B., 2014. Induction of bacterial antigen-specific colitis by a simplified human microbiota consortium in gnotobiotic interleukin-10−/− mice. Infect. Immun. 82 (6), 2239–2246. https://doi.org/10.1128/IAI.01513-13.

GBD 2017 Inflammatory Bowel Disease Collaborators., 2020. The global, regional, and national burden of inflammatory bowel disease in 195 countries and territories, 1990-2017: a systematic analysis for the global burden of Disease study 2017. Lancet Gastroenterol. Hepatol. 5 (1), 17–30. https://doi.org/10.1016/S2468-1253(19)30333-4.

Geremia, A., Biancheri, P., Allan, P., Corazza, G.R., Di Sabatino, A., 2014. Innate and adaptive immunity in inflammatory bowel disease. Autoimmun. Rev. 13 (1), 3–10. https://doi.org/10.1016/j.autrev.2013.06.004.

Groll, T., Silva, M., Sarker, R.S.J., Tschurtschenthaler, M., Schnalzger, T., Mogler, C., Denk, D., Scholch, S., Schraml, B.U., Ruland, J., Rad, R., Saur, D., Weichert, W., Jesinghaus, M., Matiasek, K., Steiger, K., 2022. Comparative study of the role of interepithelial mucosal mast cells in the context of intestinal adenoma-carcinoma progression. Cancers (Basel) 14 (9). https://doi.org/10.3390/cancers14092248.

Iacucci, M., Parigi, T.L., Del Amor, R., Meseguer, P., Mandelli, G., Bozzola, A., Bazarova, A., Bhandari, P., Bisschops, R., Danese, S., De Hertogh, G., Ferraz, J.G., Goetz, M., Grisan, E., Gui, X., Hayee, B., Kiesslich, R., Lazarev, M., Panaccione, R., et al., 2023. Artificial intelligence enabled histological prediction of remission or activity and clinical outcomes in ulcerative colitis. Gastroenterology 164 (7), 1180–1188 e1182. https://doi.org/10.1053/j.gastro.2023.02.031.

Jostins, L., Ripke, S., Weersma, R.K., Duerr, R.H., McGovern, D.P., Hui, K.Y., Lee, J.C., Schumm, L.P., Sharma, Y., Anderson, C.A., Essers, J., Mitrovic, M., Ning, K., Cleynen, I., Theatre, E., Spain, S.L., Raychaudhuri, S., Goyette, P., Wei, Z., et al., 2012. Host-microbe interactions have shaped the genetic architecture of inflammatory bowel disease. Nature 491 (7422), 119–124. https://doi.org/10.1038/nature11582.

Kappelman, M.D., Farkas, D.K., Long, M.D., Erichsen, R., Sandler, R.S., Sorensen, H.T., Baron, J.A., 2014. Risk of cancer in patients with inflammatory bowel diseases: a nationwide population-based cohort study with 30 years of follow-up evaluation. Clin. Gastroenterol. Hepatol. 12 (2), 265–273 e261. https://doi.org/10.1016/j.cgh.2013.03.034.

Katakura, K., Lee, J., Rachmilewitz, D., Li, G., Eckmann, L., Raz, E., 2005. Toll-like receptor 9-induced type I IFN protects mice from experimental colitis. J. Clin. Invest. 115 (3), 695–702. https://doi.org/10.1172/JCI22996.

Khor, B., Gardet, A., Xavier, R.J., 2011. Genetics and pathogenesis of inflammatory bowel disease. Nature 474 (7351), 307–317. https://doi.org/10.1038/nature10209.

Mahler, M., Leiter, E.H., 2002. Genetic and environmental context determines the course of colitis developing in IL-10-deficient mice. Inflamm. Bowel Dis. 8 (5), 347–355. https://doi.org/10.1097/00054725-200209000-00006.

Maschmeyer, P., Zimmermann, J., Kuhl, A.A., 2021. Murine T-cell transfer colitis as a model for inflammatory Bowel disease. Methods Mol. Biol. 2285, 349–373. https://doi.org/10.1007/978-1-0716-1311-5_26.

Medzhitov, R., 2008. Origin and physiological roles of inflammation. Nature 454 (7203), 428–435. https://doi.org/10.1038/nature07201.

Medzhitov, R., 2010. Inflammation 2010: new adventures of an old flame. Cell 140 (6), 771–776. https://doi.org/10.1016/j.cell.2010.03.006.

Mentella, M.C., Scaldaferri, F., Pizzoferrato, M., Gasbarrini, A., Miggiano, G.A.D., 2020. Nutrition, IBD and gut microbiota: a review. Nutrients 12 (4). https://doi.org/10.3390/nu12040944.

Meyerholz, D.K., Beck, A.P., 2018. Fundamental concepts for Semiquantitative tissue scoring in translational research. ILAR J. 59 (1), 13–17. https://doi.org/10.1093/ilar/ily025.

Munkholm, P., 2003. Review article: the incidence and prevalence of colorectal cancer in inflammatory bowel disease. Aliment. Pharmacol. Ther. 18 (Suppl. 2), 1–5. https://doi.org/10.1046/j.1365-2036.18.s2.2.x.

Nolte, T., Brander-Weber, P., Dangler, C., Deschl, U., Elwell, M.R., Greaves, P., Hailey, R., Leach, M.W., Pandiri, A.R., Rogers, A., Shackelford, C.C., Spencer, A., Tanaka, T., Ward, J.M., 2016. Nonproliferative and proliferative lesions of the gastrointestinal tract, pancreas and salivary glands of the rat and mouse. J. Toxicol. Pathol. 29 (1 Suppl), 1S–125S. https://doi.org/10.1293/tox.29.1S.

Peyrin-Biroulet, L., Adsul, S., Stancati, A., Dehmeshki, J., Kubassova, O., 2024. An artificial intelligence-driven scoring system to measure histological disease activity in ulcerative colitis. United European Gastroenterol J. https://doi.org/10.1002/ueg2.12562.

Pillay, J., Tak, T., Kamp, V.M., Koenderman, L., 2013. Immune suppression by neutrophils and granulocytic myeloid-derived suppressor cells: similarities and differences. Cell. Mol. Life Sci. 70 (20), 3813–3827. https://doi.org/10.1007/s00018-013-1286-4.

Rath, E., Haller, D., 2022. Intestinal epithelial cell metabolism at the interface of microbial dysbiosis and tissue injury. Mucosal Immunol. 15 (4), 595–604. https://doi.org/10.1038/s41385-022-00514-x.

Saez, A., Herrero-Fernandez, B., Gomez-Bris, R., Sanchez-Martinez, H., Gonzalez-Granado, J.M., 2023. Pathophysiology of Inflammatory Bowel Disease: innate immune system. Int. J. Mol. Sci. 24 (2). https://doi.org/10.3390/ijms24021526.

Schirmer, M., Garner, A., Vlamakis, H., Xavier, R.J., 2019. Microbial genes and pathways in inflammatory bowel disease. Nat. Rev. Microbiol. 17 (8), 497–511. https://doi.org/10.1038/s41579-019-0213-6.

Sellon, R.K., Tonkonogy, S., Schultz, M., Dieleman, L.A., Grenther, W., Balish, E., Rennick, D.M., Sartor, R.B., 1998. Resident enteric bacteria are necessary for development of spontaneous colitis and immune system activation in interleukin-10-deficient mice. Infect. Immun. 66 (11), 5224–5231. https://doi.org/10.1128/IAI.66.11.5224-5231.1998.

Singh, N., Baby, D., Rajguru, J.P., Patil, P.B., Thakkannavar, S.S., Pujari, V.B., 2019. Inflammation and cancer. Ann. Afr. Med. 18 (3), 121–126. https://doi.org/10.4103/aam.aam_56_18.

Steiger, K., Ballke, S., Yen, H.Y., Seelbach, O., Alkhamas, A., Boxberg, M., Schwamborn, K., Knolle, P.A., Weichert, W., Mogler, C., 2019. Histopathological research laboratories in translational research : conception and integration into the infrastructure of pathological institutes. Pathologe 40 (2), 172–178. https://doi.org/10.1007/s00292-018-0458-2 (Histopathologische Forschungslabors in der translationalen Forschung : Konzeption sowie Integration in die Infrastruktur pathologischer Institute.).

Uchikov, P., Khalid, U., Vankov, N., Kraeva, M., Kraev, K., Hristov, B., Sandeva, M., Dragusheva, S., Chakarov, D., Petrov, P., Dobreva-Yatseva, B., Novakov, I., 2024. The role of artificial intelligence in the diagnosis and treatment of ulcerative colitis. Diagnostics (Basel) 14 (10). https://doi.org/10.3390/diagnostics14101004.

Urbauer, E., Aguanno, D., Mindermann, N., Omer, H., Metwaly, A., Krammel, T., Faro, T., Remke, M., Reitmeier, S., Barthel, S., Kersting, J., Huang, Z., Xian, F., Schmidt, M., Saur, D., Huber, S., Stecher, B., List, M., Gomez-Varela, D., et al., 2024. Mitochondrial perturbation in the intestine causes microbiota-dependent injury and gene signatures discriminative of inflammatory disease. Cell Host Microbe. https://doi.org/10.1016/j.chom.2024.06.013.

Waldner, M.J., Neurath, M.F., 2009. Chemically induced mouse models of colitis. Curr Protoc Pharmacol. https://doi.org/10.1002/0471141755.ph0555s46. Chapter 5, Unit 5 55.

Wang, S.L., Shao, B.Z., Zhao, S.B., Chang, X., Wang, P., Miao, C.Y., Li, Z.S., Bai, Y., 2019. Intestinal autophagy links psychosocial stress with gut microbiota to promote inflammatory bowel disease. Cell Death Dis. 10 (6), 391. https://doi.org/10.1038/s41419-019-1634-x.

Ward, J.M., 2006. Lymphomas and leukemias in mice. Exp. Toxicol. Pathol. 57 (5–6), 377–381. https://doi.org/10.1016/j.etp.2006.01.007.

Ward, J.M., Erexson, C.R., Faucette, L.J., Foley, J.F., Dijkstra, C., Cattoretti, G., 2006. Immunohistochemical markers for the rodent immune system. Toxicol. Pathol. 34 (5), 616–630. https://doi.org/10.1080/01926230600941340.

Ward, J.M., Rehg, J.E., Morse 3rd., H.C., 2012. Differentiation of rodent immune and hematopoietic system reactive lesions from neoplasias. Toxicol. Pathol. 40 (3), 425–434. https://doi.org/10.1177/0192623311431467.

Weiss, U., 2008. Inflammation. Nature 454 (7203), 427. https://doi.org/10.1038/454427a.

Wong, C., Harris, P.J., Ferguson, L.R., 2016. Potential benefits of dietary fibre intervention in Inflammatory Bowel Disease. Int. J. Mol. Sci. 17 (6). https://doi.org/10.3390/ijms17060919.

Yoshida, H., Kiyuna, T., 2021. Requirements for implementation of artificial intelligence in the practice of gastrointestinal pathology. World J. Gastroenterol. 27 (21), 2818–2833. https://doi.org/10.3748/wjg.v27.i21.2818.